Available online at www.sciencedirect.com
SCIENCE DIRECT
Geochimica et Cosmochimica Acta 70 (2006) 757–766
Geochimica
www.elsevier.com/locate/gca

Mg–Fe partitioning between olivine and ultramafic melts at high pressures

Kenji Mibe [a,*], Toshitsugu Fujii [a], Atsushi Yasuda [a], Shigeaki Ono [b]

[a] *Earthquake Research Institute, University of Tokyo, 1-1-1 Yayoi, Bunkyo-ku, Tokyo 113-0032, Japan*
[b] *Institute for Research on Earth Evolution, Japan Agency for Marine-Earth Science and Technology, 2-15 Natsushima-cho, Yokosuka, Kanagawa 237-0061, Japan*

Received 22 October 2004; accepted in revised form 30 September 2005

Abstract

Precise determination of the partitioning of Mg and Fe^{2+} between olivine and ultramafic melt has been made at pressures from 5 to 13 GPa using a MA-8 type multi-anvil high-pressure apparatus (PREM) installed at Earthquake Research Institute, University of Tokyo. A very short rhenium capsule (<100 μm sample thickness) was adopted to minimize temperature variation within the sample container. Synthetic gels with the composition of the upper mantle peridotite were used as starting materials to promote the homogeneity. Analyses of quenched melts and coexisting olivines were made with an electron probe microanalyzer. The obtained partition coefficient, K_D [=$(FeO/MgO)^{ol}/(FeO/MgO)^{melt}$], decreases from 0.35 to 0.25 with increasing pressure from 5 to 13 GPa, suggesting a negative correlation between pressure and K_D above 5 GPa. Our result is consistent with a parabolic relationship between K_D and degree of polymerization (NBO/T) of melts reported by previous studies at lower pressures. The negative correlation between pressure and K_D suggests that olivine crystallizing in a magma ocean becomes more Mg-rich with depth and that primary magmas generated in the upper mantle become more Fe-rich with depth than previously estimated.

1. Introduction

Mg–Fe^{2+} partitioning between olivine and melt provides useful information on magmatism and chemical differentiation in the Earth's interior (e.g., Roeder and Emslie, 1970). Many workers have shown that the molar partition coefficient, $K_D = (FeO/MgO)^{ol}/(FeO/MgO)^{melt}$, is a function of pressure, temperature, and composition of melt (e.g., Longhi et al., 1978; Takahashi, 1978; Ford et al., 1983; Takahashi and Kushiro, 1983; Gee and Sacks, 1988; Ulmer, 1989; Baker et al., 1995; Kushiro and Walter, 1998; Xirouchakis et al., 2001; Kushiro and Mysen, 2002). Takahashi and Kushiro (1983) and Ulmer (1989) reported positive pressure dependence of K_D in peridotitic and basaltic systems up to about 4 GPa. At higher pressures nearly constant K_Ds have been observed in experimental melting of peridotite up to about 15 GPa (Takahashi, 1986; Agee and Walker, 1988a; Herzberg and Zhang, 1996).

Recently, Kushiro and Walter (1998) and Kushiro and Mysen (2002) reported a parabolic relationship between K_D and degree of polymerization, parameterized as non-bridging oxygen/tetrahedrally coordinated cations (NBO/T, see Mysen et al., 1982), of melts. K_D increases with increasing NBO/T from 0 to ~2, and then decreases with increasing NBO/T from ~2 to 4 (Kushiro and Walter, 1998). In general, NBO/T of melts generated by the partial melting of mantle peridotite increases monotonically with increasing pressure (e.g., Kushiro and Walter, 1998; Gaetani, 2004). Therefore, if the studies by Kushiro and Walter (1998) and Kushiro and Mysen (2002) are correct, then a negative correlation between pressure and K_D is expected at high pressure where NBO/T of melt becomes larger than 2. On the contrary, if K_D becomes nearly constant above 5 GPa as reported by Takahashi (1986) Agee and Walker

* Corresponding author. Present address: Department of Earth and Atmospheric Sciences, Cornell University, Snee Hall, Ithaca, NY 14853-1504, USA. Fax: +1 607 254 4780.
E-mail address: mibe@eri.u-tokyo.ac.jp (K. Mibe).

0016-7037/$ - see front matter © 2005 Elsevier Inc. All rights reserved.
doi:10.1016/j.gca.2005.09.022

(1988a), and Herzberg and Zhang (1996), then nearly constant K_D with respect to NBO/T from ~2 to 4 should be observed because NBO/T of melts obtained by these studies is larger than 2. Here, we report new determinations of the olivine–melt K_D for mantle peridotite compositions at pressures from 5 to 13 GPa, obtained in melting experiments with low thermal gradients, and discuss the implications for magmatism and chemical differentiation in the Earth's interior.

2. Experiments

2.1. Experimental procedure

The composition of the starting material used in the present study, shown in Table 1, is similar in composition to peridotite KLB-1 (Takahashi, 1986) and the model upper mantle peridotite composition, pyrolite, proposed by Ringwood (1966). Synthetic gels were used as starting materials because gels are more homogeneous and reactive than oxide mixes and therefore rapidly reach equilibrium (Hamilton and Henderson, 1968; Ono, 1998). Reagent-grade Fe, Ni, Mn, Al, MgO, CrO_3, $CaCO_3$, Na_2CO_3, and K_2CO_3 were weighed in the desired proportions and dissolved in nitric acid. The solution was then mixed with alcoholic solutions of $(C_2H_5O)_4Si$ and $(C_3H_7O)_4Ti$ in the desired ratios. The gels were precipitated from solution by hydrolysis with ammonium hydroxide. The precipitated gels were then dried and heated at 600–700 °C for about 1 h. After being ground, the gels were heated again at 950 °C for 2 h at an oxygen fugacity of the quartz–fayalite–magnetite (QFM) buffer. The composition of the gel thus prepared was determined by X-ray fluorescence (XRF) at the Earthquake Research Institute, University of Tokyo (Nakada, 1997), using a glass bead with 10 parts flux to one part sample.

Table 1
Composition of starting material (wt%)

	This study (XRF)	This study (EPMA)	KLB-1	Pyrolite
SiO_2	45.41 (15)[a]	45.70 (39)[b]	44.48	45.20
TiO_2	0.18 (01)	0.16 (02)	0.16	0.71
Al_2O_3	3.30 (11)	3.24 (14)	3.59	3.54
Cr_2O_3	0.45 (02)	0.48 (02)	0.31	0.43
FeO	8.17 (67)	7.59 (26)	8.10	8.47
MnO	0.12 (01)	0.12 (38)	0.12	0.14
MgO	38.25 (40)	38.88 (38)	39.22	37.50
NiO	0.29 (01)	0.14 (02)	0.25	0.20
CaO	3.56 (12)	3.47 (17)	3.44	3.08
Na_2O	0.25 (01)	0.21 (02)	0.30	0.57
K_2O	0.02 (01)	0.01 (01)	0.02	0.13
P_2O_5	—	—	0.03	0.04
Total	100.00	100.00	100.02	100.01
Mg#[c]	89.3	90.1	89.6	88.8

KLB-1, spinel lherzolite from Kilbourne Hole crater (Takahashi, 1986); Pyrolite, Hawaiian pyrolite (Ringwood, 1966).
[a] Estimated errors for XRF analysis (the last digits).
[b] Two standard errors of the mean ($2\sigma/\sqrt{n}$) of 16 analyses.
[c] Mg# calculated as molar 100Mg/(Mg + Fe).

High pressure and high temperature experiments were carried out using a Kawai-type multi-anvil high-pressure apparatus (PREM) installed at the Earthquake Research Institute, University of Tokyo (Mibe et al., 2003). Tungsten carbide (WC) cubic anvils with 12-, 8-, and 4-mm corner truncation edge lengths were used for pressures up to 5, 10, and 13 GPa, respectively. Semi-sintered ZrO_2 octahedron pressure medium and a cylindrical graphite heater were used in the experiments at 5 GPa, whereas semi-sintered MgO (+5 wt% Cr_2O_3) octahedron pressure medium and a cylindrical $LaCrO_3$ heater were used in the experiments at higher pressures. Mo foil was used as electrodes. The gel starting material was put in a Re capsule (Figs. 1A and B). The thickness of the sample layer is about 100 μm (Fig. 2A) except for run no. 1102 (see Section 3). In order to investigate the effect of fO_2 on K_D, two runs were done at 5 GPa using graphite sample capsule (Table 2). The thickness of the sample in the graphite capsule is about 200 μm and the experimental configuration is the same as Fig. 2A. The pressure media and all of the ceramics parts, except for the capsules, were fired for 1 h at 1000 °C before assembly. After assembly, they were kept in a vacuum oven for more than 3 h at 160 °C until just before experiments to ensure near-anhydrous run conditions.

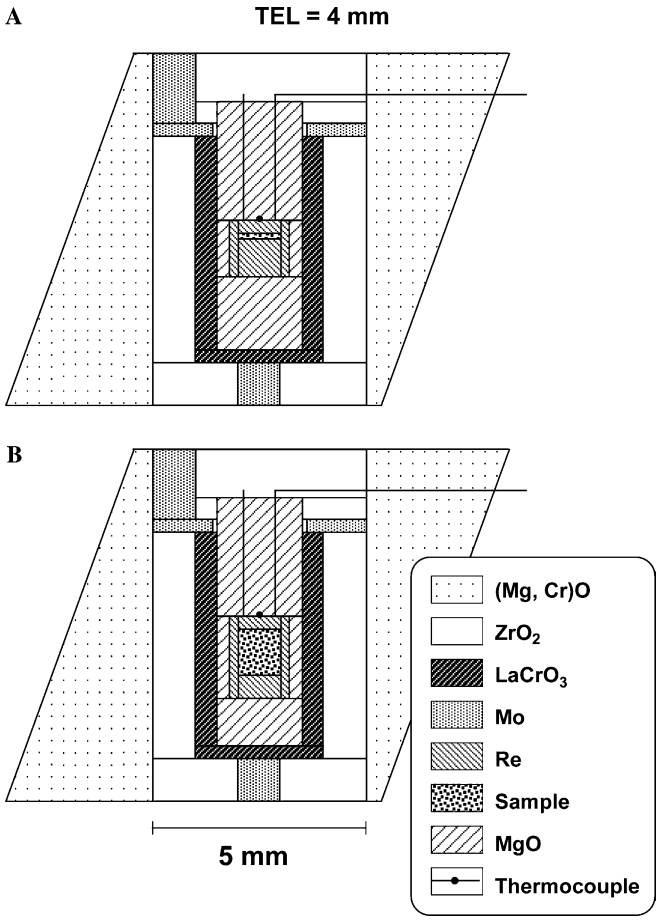

Fig. 1. Furnace assemblies used in the present study. (A) For all the runs except for run no. 1102. (B) For run no. 1102.

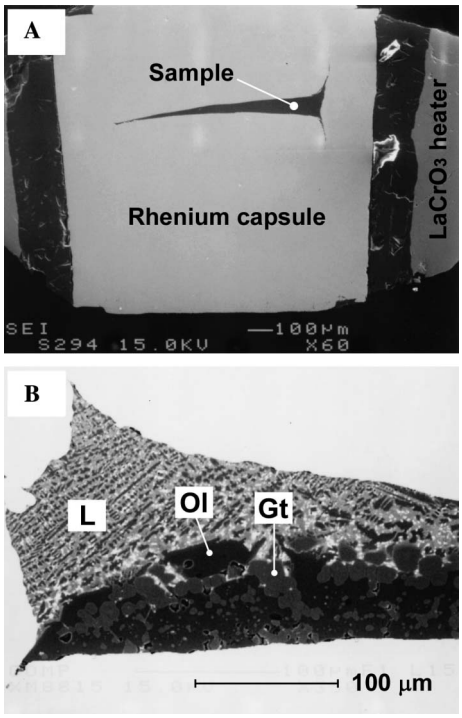

Fig. 2. (A) Secondary electron image of a recovered sample (Run no. 1101). (B) Backscattered electron image of a recovered sample (Run no. 1201). Note that the height of the sample in (A) is about 100 μm.

Table 2
Conditions of high pressure experiments

Run no.	P (GPa)	T (°C)	Duration (min)	Capsule[a]	Phases[b]
0503	5	1750	20	Re	Ol (43.7) + L (56.0)
0504	5	1750	25	Re	Ol (37.2) + L (62.5)
0505	5	1750	20	C	Ol (35.2) + L (66.7)
0506	5	1750	20	C	Ol (37.7) + L (62.7)
0802	8	1850	90	Re	Ol (22.9) + L (77.0)
0804	8	1900	15	Re	Ol (16.2) + L (83.8)
1001	10	1950	15	Re	Ol (27.4) + L (72.1)
1002	10	2000	15	Re	Ol (14.4) + L (85.8)
1101	11	2000	15	Re	Ol + Gt + L (n.a.)[d]
1102	11	2000	10	Re[c]	Ol + Gt + Cpx + L (n.a.)
1207	12	1900	45	Re	Ol (41.2) + Gt (37.9) + L (21.2)
1202	12	2000	30	Re	Ol (31.8) + Gt (28.1) + L (40.7)
1201	12	2020	25	Re	Ol (12.1) + Gt (8.2) + L (79.6)
1301	13	2000	30	Re	Ol (13.7) + Gt (17.6) + L (69.2)
1604	16	2100	15	Re	L (100)

[a] Re, rhenium; C, graphite.
[b] L, liquid; Ol, olivine; Gt, garnet; Cpx, clinopyroxene. Numbers in parentheses indicate modal abundances of phases (wt%).
[c] Large capsule (~1 mm height).
[d] n.a., not analyzed.

The temperature of the samples was monitored with a W3%Re–W25%Re thermocouple. Because thermocouple emf signals were conducted through the surface of the tungsten carbide cubes to the temperature measurement electronics, it was necessary to make a correction for the surface temperature of the anvils. This was done by attaching a chromel–alumel thermocouple to the anvil surface (e.g., Irifune and Ohtani, 1986). A correction for the effect of pressure on the thermocouple emf was not applied. The relationship between load and sample pressure was calibrated using the following phase transformations; Mg_2SiO_4 (α–β) at 1600 °C and 15.1 GPa (Morishima et al., 1994); Mg_2SiO_4 (β–γ) at 1300 °C and 18.9 GPa, and at 1400 °C and 19.4 GPa (Akaogi et al., 1989). The uncertainties in pressure and temperature are estimated to be about ±0.4 GPa and ±20 °C, respectively.

The experiments were run at pressures from 5 to 13 GPa and at temperatures from 1750 to 2020 °C (Table 2). Pressure was applied first and then temperature was increased to the desired value. The sample was held at a constant temperature and pressure for 15–90 min. During experiments, temperature was controlled within ±3 °C of the desired value. After the run, the charge was quenched by shutting off the power supply without changing the load. After pressure was released, the sample was recovered.

The charges were mounted in epoxy and polished. Then chemical composition was analyzed by WDS with a five-spectrometer JEOL JXA-8800 electron probe microanalyzer (EPMA) at the Earthquake Research Institute, University of Tokyo. The data were reduced using the correction procedure of Bence and Albee (1968). An acceleration voltage of 15 kV and a beam current of 12 nA were employed. Counting time was 10 s for all elements. A focused electron beam was employed for analysis of minerals. A 15–20 μm diameter electron beam was used to obtain melt composition because the melt cannot be quenched into a homogeneous glass, but rather forms a dendritic intergrowth of quench crystals (Fig. 2B). In order to check the validity of the broad beam probe analysis of the quenched crystals, we conducted a superliquidus experiment at 16 GPa. The average composition of 16 points is listed in Table 1 and is in good agreement with XRF analysis, although some amounts of FeO and NiO have lost as a result of diffusion into the Re capsule. Fe^{3+}/Fe^{2+} of melts was not determined because of the difficulty in determining these elemental ratios in the dendritic quench crystals. K_D was, therefore, calculated on the assumption that Fe in melt is all Fe^{2+}. In addition to the graphite runs, the effect of fO_2 on the K_D was also examined by estimating Fe_2O_3 content in the liquid by mass balance calculations (see Section 4). All the chemical analyses (EPMA and XRF) shown in tables are normalized to 100 wt%.

3. Results

The phase assemblages of the recovered run products are listed in Table 2. The average grain size of olivine and garnet is about 20 and 10 μm, respectively. According to Chakraborty et al. (1999), Mg–Fe inter-diffusion rate in olivine when extrapolated to temperature of 2000 °C is about 10^{-13} m^2/s. The diffusive-mixing time scale (given by $r^2/D \sim t$, where r is the radius of olivine grain, D is the diffusion coefficient, and t is the time) for homogenizing 20 mm (diameter) olivine is about 15 min. Therefore, the

experimental duration in the present study is thought to be sufficient to attain equilibrium. EPMA analyses showed that olivine is homogeneous (Table 3) and does not show detectable compositional zoning (see olivines no. 11 and 12 in Fig. 4), consistent with chemical equilibrium being attained in all sample charges except for the run no. 1102 (see Section 3).

Most of the previous high-pressure melting studies using multi-anvil apparatus have suffered from the presence of large temperature gradients. With large temperature gradients present, attainment of chemical equilibrium can be prevented by several complex physicochemical processes, such as Soret diffusion, saturation gradient chemical diffusion (Lesher and Walker, 1988), and cold-directed thermal migration (Herzberg and Zhang, 1996). As a result of these effects, an equilibrium K_D cannot be determined precisely. To minimize temperature gradients, therefore, we reduced the sample thickness to 100 μm (Fig. 1A).

The effect of temperature gradients on K_D was examined by changing the sample thickness under the same pressure and temperature condition. Two runs were done at 11 GPa and 2000 °C (runs 1101 and 1102). Run no. 1101 has sample thickness of about 100 μm (Fig. 1A), whereas the sample thickness of run 1102 was about 1 mm (Fig. 1B). In general, the central part of the furnace assembly has smaller temperature gradient than the outer part, and the gradient is steeper in axial direction along to the heater (e.g., Gasparik, 1996) than in horizontal direction in Fig. 1. The temperature differences between the hottest part and the coldest part of the samples in runs 1101 (100 μm) and 1102 (1 mm) were estimated to be less than 20 °C and more than 100 °C, respectively. The phase assemblage in the recovered sample charge of the run 1101 is olivine + garnet + melt. A similar assemblage is observed in run 1102 except with the addition of clinopyroxene in the coldest part of the charge (Table 2). Olivine is distributed over almost the entire area from the hotter part to the colder end in the capsule of run 1102. Compositions of the melts in the two runs, 1101 and 1102, are the same within uncertainty, except for Na_2O (Table 4). Melts in both runs are homogeneous and there is no compositional difference between the melts in the hotter part and colder end, indicating Soret diffusion is undetectable in our experiments. The composition of olivine in run 1101 is also homogeneous. In contrast, the compositional range of olivine (especially FeO and MgO) in run 1102 is extremely large when compared to other runs

Table 3
Compositions of minerals (wt%)

Run no.	0503	0504	0505	0506	0802	0804	1001	1002	1101
Phase	Ol	Ol	Ol	Ol	Ol	Ol	Ol	Ol	Ol
n^a	18	10	9	24	21	22	29	11	12
SiO_2	40.98 (0.38)	41.04 (0.25)	40.79 (0.31)	40.92 (0.33)	41.09 (0.18)	40.98 (0.30)	41.12 (0.28)	41.15 (0.17)	41.00 (0.36)
TiO_2	0.01 (0.03)	0.01 (0.04)	0.00 (0.01)	0.01 (0.03)	0.01 (0.02)	0.01 (0.02)	0.01 (0.02)	0.00 (0.01)	0.01 (0.04)
Al_2O_3	0.14 (0.04)	0.12 (0.02)	0.25 (0.26)	0.18 (0.07)	0.17 (0.04)	0.16 (0.04)	0.15 (0.07)	0.19 (0.04)	0.14 (0.03)
Cr_2O_3	0.23 (0.06)	0.24 (0.07)	0.27 (0.07)	0.26 (0.06)	0.14 (0.07)	0.12 (0.06)	0.11 (0.07)	0.09 (0.03)	0.07 (0.06)
FeO	5.32 (0.26)	4.50 (0.18)	5.46 (0.28)	5.45 (0.36)	4.38 (0.20)	4.12 (0.20)	4.25 (0.35)	3.44 (0.14)	4.28 (0.26)
MnO	0.07 (0.05)	0.06 (0.05)	0.09 (0.04)	0.07 (0.05)	0.06 (0.04)	0.06 (0.04)	0.06 (0.04)	0.05 (0.06)	0.06 (0.05)
MgO	52.94 (0.26)	53.88 (0.40)	52.88 (0.61)	52.92 (0.39)	53.91 (0.32)	54.07 (0.32)	53.77 (0.33)	54.66 (0.25)	53.92 (0.48)
NiO	0.17 (0.09)	0.03 (0.04)	0.02 (0.05)	0.03 (0.04)	0.12 (0.07)	0.37 (0.06)	0.38 (0.05)	0.30 (0.08)	0.38 (0.07)
CaO	0.14 (0.04)	0.12 (0.03)	0.24 (0.12)	0.16 (0.03)	0.12 (0.04)	0.11 (0.04)	0.15 (0.03)	0.12 (0.04)	0.14 (0.04)
Na_2O	—	—	—	—	—	—	—	—	—
Total	100.00	100.00	100.00	100.00	100.00	100.00	100.00	100.00	100.00
Mg#	94.7	95.5	94.5	94.5	95.6	95.9	95.8	96.6	95.7

Run no.	1102	1207		1202		1201		1301	
Phase	Ol	Ol	Gt	Ol	Gt	Ol	Gt	Ol	Gt
n^a	80	14	8	18	11	12	9	16	11
SiO_2	40.81 (0.45)	40.97 (0.20)	51.14 (1.16)	41.04 (0.22)	50.77 (0.63)	41.15 (0.43)	50.24 (0.75)	41.22 (0.21)	51.04 (0.42)
TiO_2	0.01 (0.02)	0.01 (0.04)	0.14 (0.09)	0.01 (0.02)	0.09 (0.05)	0.00 (0.02)	0.04 (0.04)	0.01 (0.03)	0.04 (0.05)
Al_2O_3	0.13 (0.15)	0.07 (0.04)	8.64 (1.78)	0.09 (0.03)	10.48 (1.52)	0.14 (0.05)	12.82 (0.91)	0.12 (0.04)	11.92 (0.45)
Cr_2O_3	0.07 (0.06)	0.06 (0.07)	1.11 (0.24)	0.07 (0.06)	1.25 (0.18)	0.08 (0.05)	1.17 (0.10)	0.05 (0.05)	1.07 (0.17)
FeO	5.12 (1.54)	5.84 (0.22)	5.48 (0.33)	4.81 (0.26)	4.22 (0.34)	3.54 (0.19)	2.79 (0.22)	3.72 (0.25)	2.71 (0.26)
MnO	0.06 (0.04)	0.07 (0.04)	0.13 (0.06)	0.07 (0.05)	0.10 (0.04)	0.06 (0.04)	0.07 (0.04)	0.05 (0.04)	0.07 (0.04)
MgO	53.20 (1.48)	52.40 (0.26)	28.61 (0.77)	53.39 (0.30)	29.61 (0.84)	54.69 (0.38)	31.23 (0.45)	54.48 (0.23)	31.61 (0.45)
NiO	0.42 (0.10)	0.36 (0.09)	0.07 (0.07)	0.32 (0.06)	0.04 (0.06)	0.22 (0.05)	0.06 (0.03)	0.21 (0.06)	0.03 (0.05)
CaO	0.18 (0.09)	0.22 (0.05)	4.57 (0.41)	0.20 (0.03)	3.38 (0.62)	0.12 (0.03)	1.52 (0.61)	0.14 (0.04)	1.48 (0.60)
Na_2O	—	—	0.11 (0.03)	—	0.06 (0.04)	—	0.04 (0.03)	—	0.03 (0.02)
Total	100.00	100.00	100.00	100.00	100.00	100.00	100.00	100.00	100.00
Mg#	94.9	94.1	90.3	95.2	92.6	96.5	95.2	96.3	95.4

Numbers in parentheses indicate two standard errors (2σ).
[a] Number of analyses.

(Table 3). This is because FeO/MgO ratio of olivine in run 1102 increases systematically from the hotter part toward the colder end as a result of the large temperature gradient.

Using the average melt compositions listed in Table 4 and individual olivine analyses, apparent K_Ds can be calculated. The number of analyses of olivine for 1101 and 1102 is 12 and 80, respectively (Table 3). Therefore, 12 and 80 apparent K_Ds were obtained for runs 1101 and 1102, respectively. A histogram of the apparent K_D distribution is shown in Fig. 3. In run 1101, the average K_D value is 0.274 (Table 4) and K_D ranges from 0.25 to 0.30 (Fig. 3). On the other hand, the K_Ds in run 1102 vary over a wide range, from 0.27 to 0.50 (Fig. 3). Propagated errors for K_D (calculated using one standard deviation for olivines and one standard error of the mean for the liquid compositions) in runs 1101 and 1102 are 0.010 and 0.051, respectively (Table 4). This wide distribution in run 1102 stems directly from the compositional variation of olivine under the large temperature gradients. In this case, the average K_D value determined for run 1102 could be larger than the equilibrium value depending on how the olivines are selected to get the average composition. The average of 80 K_Ds in the run 1102 is 0.335 (Table 4), which is much larger than the average K_D for the run 1101 ($K_D = 0.274$) although these two runs were run at the same pressure and temperature conditions. These results indicate that minimizing the thermal gradient over the length of the capsule is important and that the equilibrium K_D can only be obtained by using a small sample container, in which case both olivine and melt are homogeneous. The spatial

Table 4
Compositions of liquid (wt%)

Run no.	0503	0504	0505	0506	0802	0804	1001
n[a]	23	32	24	86	29	29	40
SiO_2	50.11 (0.84)	49.63 (0.89)	46.06 (1.20)	48.09 (0.60)	47.34 (0.35)	46.31 (0.57)	47.52 (0.46)
TiO_2	0.30 (0.06)	0.32 (0.07)	0.29 (0.11)	0.27 (0.03)	0.13 (0.01)	0.21 (0.03)	0.23 (0.02)
Al_2O_3	5.86 (0.49)	5.41 (0.59)	5.94 (1.18)	5.76 (0.47)	4.35 (0.21)	4.21 (0.36)	3.86 (0.35)
Cr_2O_3	0.67 (0.03)	0.61 (0.04)	0.64 (0.07)	0.60 (0.02)	0.59 (0.02)	0.56 (0.04)	0.51 (0.04)
FeO	8.50 (0.26)	7.66 (0.11)	8.92 (0.30)	8.74 (0.15)	8.46 (0.17)	8.59 (0.26)	9.22 (0.20)
MnO	0.15 (0.01)	0.14 (0.01)	0.16 (0.01)	0.14 (0.01)	0.14 (0.01)	0.13 (0.01)	0.15 (0.01)
MgO	28.31 (1.60)	30.71 (2.43)	30.73 (4.12)	30.21 (1.80)	34.37 (0.79)	35.47 (1.54)	33.03 (1.11)
NiO	0.05 (0.01)	0.02 (0.01)	0.01 (0.01)	0.01 (0.00)	0.09 (0.01)	0.26 (0.02)	0.25 (0.02)
CaO	5.57 (0.50)	5.08 (0.86)	6.74 (1.68)	5.57 (0.52)	4.26 (0.22)	3.93 (0.36)	4.81 (0.28)
Na_2O	0.42 (0.04)	0.37 (0.06)	0.46 (0.11)	0.56 (0.06)	0.24 (0.01)	0.31 (0.03)	0.39 (0.03)
K_2O	0.04 (0.01)	0.04 (0.01)	0.05 (0.03)	0.05 (0.01)	0.01 (0.00)	0.02 (0.00)	0.02 (0.00)
Total	100.00	100.00	100.00	100.00	100.00	100.00	100.00
K_D	0.335 (14)	0.334 (15)	0.356 (26)	0.355 (16)	0.330 (9)	0.315 (11)	0.283 (13)
K_D[b]	0.396	0.395	—	—	0.372	0.351	0.318
NBO/T	1.86	1.98	2.19	2.05	2.34	2.45	2.34
D_{MgO}	1.870 (53)	1.755 (70)	1.720 (116)	1.752 (53)	1.568 (19)	1.524 (33)	1.627 (28)
D_{FeO}	0.626 (18)	0.587 (12)	0.612 (19)	0.623 (21)	0.518 (13)	0.480 (14)	0.460 (20)

Run no.	1002	1101	1102	1207	1202	1201	1301
n[a]	31	52	35	10	21	28	17
SiO_2	46.12 (0.55)	46.80 (0.48)	46.30 (0.39)	44.72 (0.97)	44.98 (0.39)	45.84 (0.35)	44.65 (0.31)
TiO_2	0.20 (0.02)	0.24 (0.02)	0.24 (0.02)	0.42 (0.07)	0.32 (0.03)	0.15 (0.01)	0.21 (0.02)
Al_2O_3	4.08 (0.39)	2.99 (0.23)	2.83 (0.26)	1.04 (0.17)	1.60 (0.14)	2.83 (0.19)	2.14 (0.15)
Cr_2O_3	0.53 (0.04)	0.45 (0.03)	0.41 (0.03)	0.21 (0.04)	0.33 (0.03)	0.45 (0.02)	0.43 (0.03)
FeO	8.53 (0.30)	9.84 (0.24)	9.96 (0.23)	13.60 (1.17)	11.81 (0.61)	9.04 (0.20)	10.11 (0.32)
MnO	0.13 (0.01)	0.15 (0.01)	0.15 (0.01)	0.18 (0.03)	0.17 (0.01)	0.14 (0.01)	0.15 (0.01)
MgO	35.78 (1.63)	33.93 (1.15)	34.62 (0.89)	30.29 (1.99)	33.26 (0.72)	36.82 (0.62)	36.89 (0.56)
NiO	0.25 (0.02)	0.28 (0.02)	0.30 (0.01)	0.27 (0.04)	0.26 (0.01)	0.23 (0.02)	0.20 (0.02)
CaO	4.08 (0.39)	5.02 (0.33)	4.84 (0.30)	8.57 (0.95)	6.80 (0.27)	4.24 (0.14)	5.03 (0.22)
Na_2O	0.29 (0.03)	0.29 (0.02)	0.36 (0.03)	0.65 (0.08)	0.46 (0.04)	0.25 (0.02)	0.18 (0.03)
K_2O	0.01 (0.00)	0.01 (0.00)	0.01 (0.00)	0.04 (0.01)	0.01 (0.01)	0.01 (0.00)	0.01 (0.00)
Total	100.00	100.00	100.00	100.00	100.00	100.00	100.00
K_D	0.264 (9)	0.274 (10)	0.335 (51)	0.248 (14)	0.254 (10)	0.264 (6)	0.249 (9)
K_D[b]	0.294	—	—	0.302	0.291	0.294	0.276
NBO/T	2.49	2.52	2.60	2.87	2.84	2.69	2.90
D_{MgO}	1.527 (35)	1.588 (28)	1.536 (29)	1.729 (57)	1.605 (18)	1.485 (13)	1.477 (12)
D_{FeO}	0.403 (11)	0.435 (14)	0.514 (78)	0.429 (20)	0.407 (15)	0.392 (9)	0.368 (14)

Numbers in parentheses for oxides indicate two standard errors of the mean ($2\sigma/\sqrt{n}$). Propagated errors for K_D, D_{MgO}, and D_{FeO} are calculated using one standard deviation for olivines and one standard error of the mean for the liquid compositions and refer to the last digit(s).

[a] Number of analyses.

[b] K_D values are corrected by estimating FeO and Fe_2O_3 contents in the liquid (see text for detail).

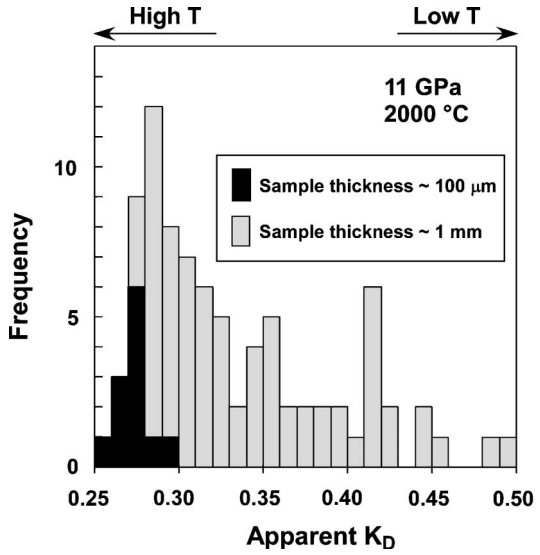

Fig. 3. Variation of apparent K_D values in the runs 1101 (black bars) and 1102 (gray bars). The apparent K_D values are calculated by dividing the compositions of individual olivine grain analyses by the melt composition in the run. Note that the apparent K_D in run 1101 varies within a narrow range. On the other hand, the distribution of the apparent K_D in run 1102 is extremely wide, indicating that chemical equilibrium has not been attained in this run.

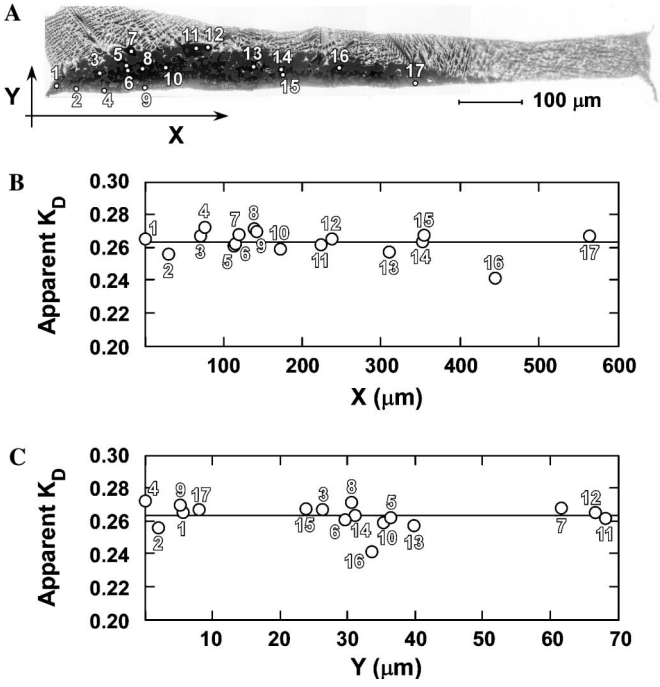

Fig. 4. The spatial variation of the K_D in run 1201. (A) Backscattered electron image showing the analyzed points. (B) The spatial variation along the *X*-axis. (C) The spatial variation along the *Y*-axis. The horizontal lines in (B) and (C) represent the average K_D value of 0.264.

variation of the K_D in run 1201 (12 GPa, 2020 °C) is shown in Fig. 4. There is no correlation between K_D and *X*-distance or *Y*-distance, indicating olivines in the entire capsule are homogeneous. Therefore, all the runs except for 1102 were conducted using a small sample capsule, with a sample thickness of about 100 μm, and the K_D was determined by dividing the average FeO/MgO of olivine by that of melt (Table 4).

4. Discussion

K_D values obtained in the present study are listed in Table 4 and plotted as a function of pressure in Fig. 5A along with data of previous peridotite melting experiments (Kushiro, 1996; Herzberg and Zhang, 1996; Walter, 1998; Taura et al., 1998; Gudfinnsson and Presnall, 2000). K_D increases with increasing pressure up to around 5 GPa as shown in a peridotitic system by Takahashi and Kushiro (1983) and in a basaltic system by Ulmer (1989). Above 5 GPa, nearly constant K_D against pressure has been reported by several workers (e.g., Takahashi, 1986; Agee and Walker, 1988a; Herzberg and Zhang, 1996). However, a negative pressure dependence of K_D above 5 GPa is observed in the present study. K_D shows a maximum value of about 0.35 at around 5 GPa, and then decreases to about 0.25 at 13 GPa. K_D values of Herzberg and Zhang (1996) and Taura et al. (1998) are slightly higher than our results. This is probably because Herzberg and Zhang (1996) and Taura et al. (1998) used large sample capsules with a height of about 1 mm. This is clearly seen in Fig. 5A as the average K_D in run 1102 with a large sample size is the same as that found by Herzberg and Zhang (1996) using large capsules. Our small capsule data points at 5 GPa are consistent with the data of Walter (1998), which were obtained by using a furnace assembly with a stepped heater that reduced temperature gradients.

What can cause the reduction of K_D with increasing pressure above 5 GPa? Previous studies have shown that ~10 wt% alkalis (e.g., Gee and Sacks, 1988; Baker et al., 1995) or ~10 wt% TiO_2 (e.g., Longhi et al., 1978; Xirouchakis et al., 2001) can cause a decrease of K_D to as low as 0.25. In the present study, however, neither alkali nor TiO_2 content in melt is high enough to decrease K_D this much. In most experiments up to 5 GPa, graphite sample capsules were used, whereas Re capsules were used in the present study. Assuming that the fO_2 in the charge is buffered by the capsule, the fO_2 in Re capsules should be higher than that in graphite capsules (Matsukage and Kubo, 2003). Therefore, the difference in capsule material could be another reason for the lowering of K_D because Fe^{3+}/Fe^{2+} of melt in Re capsules might become higher than that in graphite capsules.

To check the effect of fO_2 on K_D, two runs were done at 5 GPa using graphite capsules. Although K_Ds obtained using Re capsules (runs 0503 and 0504) are slightly smaller than those obtained using graphite capsule (runs 0505 and 0506), all of our K_Ds at 5 GPa plot within the range of data points at about 5 GPa from Walter (1998) (Fig. 5A). This indicates that the effect of capsule material is negligible, although the Fe^{3+}/Fe^{2+} of the melt is not determined in the present study. The effect of fO_2 on the K_D can be also checked by estimating Fe_2O_3 content in the liquid by mass

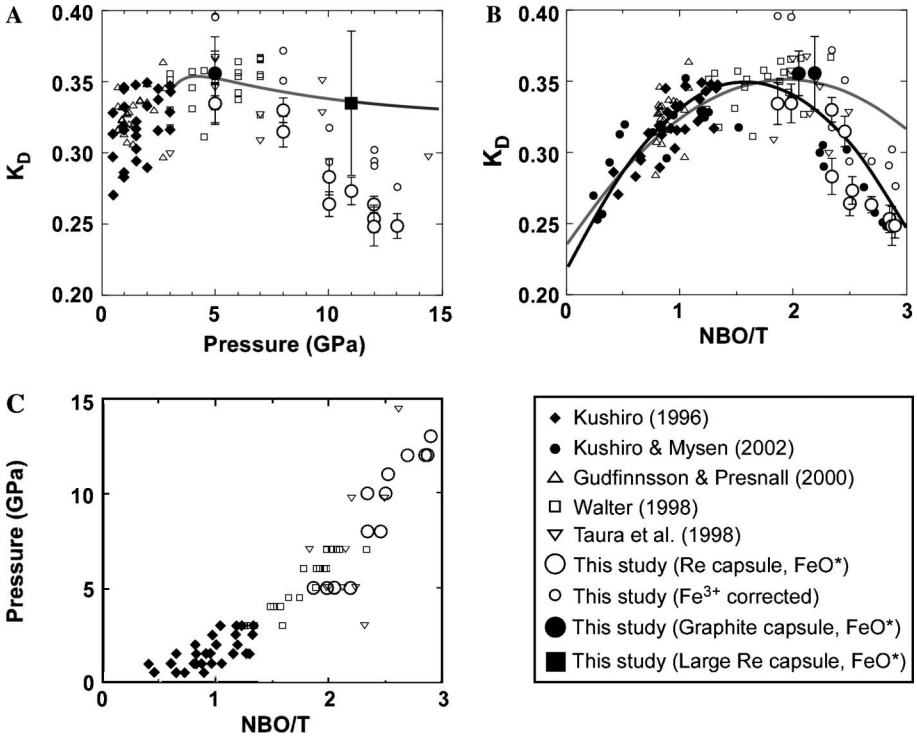

Fig. 5. Variation of K_D as a function of (A) pressure and (B) NBO/T. (C) Plot of pressure versus NBO/T of melts generated by the partial melting of mantle peridotite. The gray curves in (A) and (B) are the variation of K_D as a function of pressure reported by Herzberg and Zhang (1996) and the second-order polynomial curve obtained by Kushiro and Walter (1998), respectively. The gray curve in (A) is calculated using the pressure variation of olivine/liquid partition coefficients for FeO and MgO reported by Herzberg and Zhang (1996). The solid curve in (B) is a parabola fitted to all the data points in (B). The fitted equation relating K_D to NBO/T is given as the following: $K_D = 0.217 + 0.167 \times (\mathrm{NBO/T}) - 0.052 \times (\mathrm{NBO/T})^2$, [$R = 0.77$].

balance calculations. This is done by solving for **x** in the matrix equation, $\mathbf{A} \cdot \mathbf{x} = \mathbf{b}$, where **A** is an $M \times N$ matrix composed of M phases and N components (composition matrix), **x** is the solution vector (phase mode), and **b** is a known vector (bulk composition). The major element components SiO_2, Al_2O_3, MgO, and CaO are used for the mass balance calculation. Given a set of **A** and **b**, **x** can be calculated by least squares to minimize the difference between **b** (bulk composition of starting material) and **b**′ (calculated bulk composition). Here, we assume that (1) 10% of Fe in the starting material was present as Fe_2O_3 (a reasonable assumption for a powder reduced at QFM buffer) and is totally anhydrous, (2) that the experiment lost no Fe, and (3) that all of the Fe_2O_3 remained in the liquid, if there is no garnet. (4) If there is garnet in the recovered sample, 15% of Fe in garnet was present as Fe_2O_3 (Miyajima et al., 2004). The modal abundances obtained based on these assumptions are listed in Table 2. From these modal abundances, the corrected K_D can be calculated using FeO content in the liquid. The corrected K_D values are listed in Table 4 and are plotted in Fig. 5A. All the corrected K_D values are shifted to higher than the K_D values obtained using FeO^*. However, the negative correlation between K_D and pressure does still exist (Fig. 5A).

Instead of being caused by high fO_2, the reduction of K_D with pressure above 5 GPa could be explained by the NBO/T dependence of K_D. The variation of K_D as a function of NBO/T of the melt is shown in Fig. 5B. Besides K_Ds obtained in the present study, Fig. 5B also includes melting experiments at 1 atm (Kushiro and Mysen, 2002) and at high pressures (Kushiro, 1996; Walter, 1998; Taura et al., 1998; Gudfinnsson and Presnall, 2000). The structure of silicate melts at high pressures is known to be different from that at 1 atm because of pressure-induced change in coordination of Si and Al (e.g., Xue et al., 1991; Lee et al., 2004). However, the role of each oxide in silicate melts at high pressures is not yet completely understood. We, therefore, calculated NBO/T from the composition of melt, without considering the effect of pressure on melt structure. K_D obtained in the present study decreases from ~0.35 to ~0.25 with increasing NBO/T from ~2 to ~3. As in lower pressure experiments of Kushiro and Walter (1998) and Kushiro and Mysen (2002), the parabolic relationship between K_D and NBO/T can also be seen in the data from the experiments up to 13 GPa (Fig. 5B). K_D shows a maximum at NBO/T between 1 and 2. Despite the large difference in pressure, the K_Ds obtained at high pressures show almost the same variation as K_Ds at 1 atm by Kushiro and Mysen (2002). Since NBO/T of the melts plotted in Fig. 5B increases monotonically with increasing pressure (Fig. 5C), the horizontal axis (i.e., NBO/T) in Fig. 5B can be exchanged for pressure. Because NBO/T reaches 2 at 5 GPa (Fig. 5C) and K_D decreases with increasing NBO/T > 2 (Fig. 5B), a negative correlation between pressure and K_D above 5 GPa is expected, which is exactly what is observed in Fig. 5A.

The gray curve in Fig. 5B is a second-order polynomial curve fitted to data obtained in natural basalt–peridotite systems by Kushiro and Walter (1998). Kushiro and Mysen (2002) reported that variations of K_D at NBO/T > 1.4 in natural systems (gray curve in Fig. 5B) are different from those in synthetic systems (small solid circles in Fig. 5B). However, K_Ds obtained at high pressures in a natural system in the present study and those obtained at 1 atm in synthetic systems by Kushiro and Mysen (2002) plot in the same region in Fig. 5B. Although the dependence of K_D on NBO/T is the same in the study of Kushiro and Mysen (2002) and the present study, the dependence of the distribution coefficients for MgO and FeO between olivine and melt on NBO/T are different (Figs. 6A and B). In addition to this, K_Ds obtained in the present study deviate from the parabola of Kushiro and Walter (1998) at NBO/T > 2 (gray curve in Fig. 5B). It should be noted that the pressure and temperature of the experiments of Kushiro and Walter (1998) and ours are different. Although it is true that the parabolic relationship between K_D and the NBO/T of the melt is observed at high pressure up to 13 GPa, just the same as lower pressure studies by Kushiro and Walter (1998) and Kushiro and Mysen (2002), this does not necessarily mean that there is no pressure, temperature, and/or compositional dependence of K_D between olivine and melt. O'Neill and Eggins (2002) reported that there is a large difference between MgO and CaO in determining the activity coefficient for MoO_2 and MoO_3 in the liquid, whereas the NBO/T of the liquid does not distinguish between the effects of MgO and CaO. It is possible that the combined effect of pressure, temperature, and composition causes the coincidence of the dependence of K_D on NBO/T between the study of Kushiro and Mysen (2002) and the present study, because there is a large difference in MgO and CaO contents of the melts with 1.5 < NBO/T < 3.0 between these two studies.

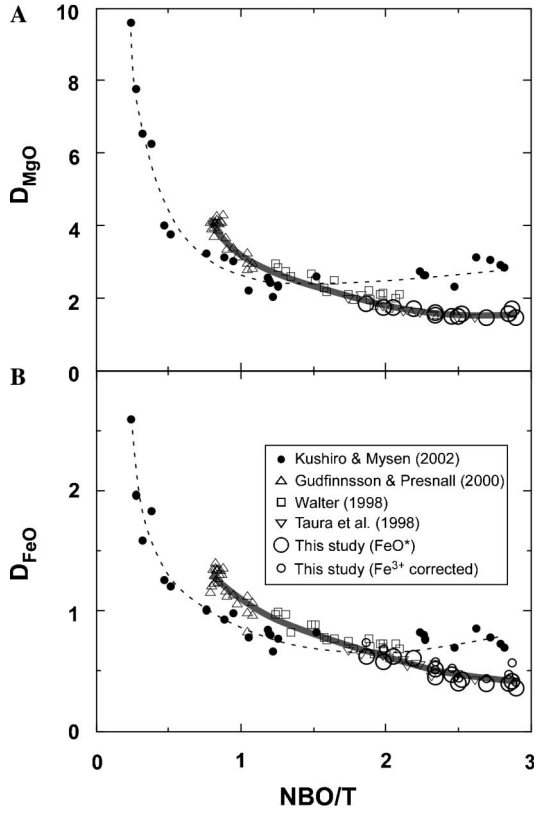

Fig. 6. Distribution coefficients for MgO ($D_{MgO} = MgO^{ol}/MgO^{melt}$) and FeO ($D_{FeO} = FeO^{ol}/FeO^{melt}$) as a function of NBO/T of melt. Gray lines: data at high pressures (drawn by hands). Dotted lines: data at 1 atm in synthetic system (after Kushiro and Mysen, 2002).

It has been pointed out that there is a linear relationship between inverse temperature and $\log D_{MgO}$ and $\log D_{FeO}$ (e.g., Roeder and Emslie, 1970; Longhi et al., 1978; Gaetani and Grove, 1998; Sugawara, 2000; Gudfinnsson and Presnall, 2001). Figs. 7A–C display plots of $\log D_{MgO}$, $\log D_{FeO}$, and $\log K_D$ vs inverse temperature. The solid lines in Figs. 7A and B represent linear regressions fitted to the data by Gudfinnsson and Presnall (2000) and Walter (1998). The data points obtained by Gudfinnsson and Presnall (2000) and Walter (1998) fit very well with a linear regression. Most of the data points by Taura et al. (1998)

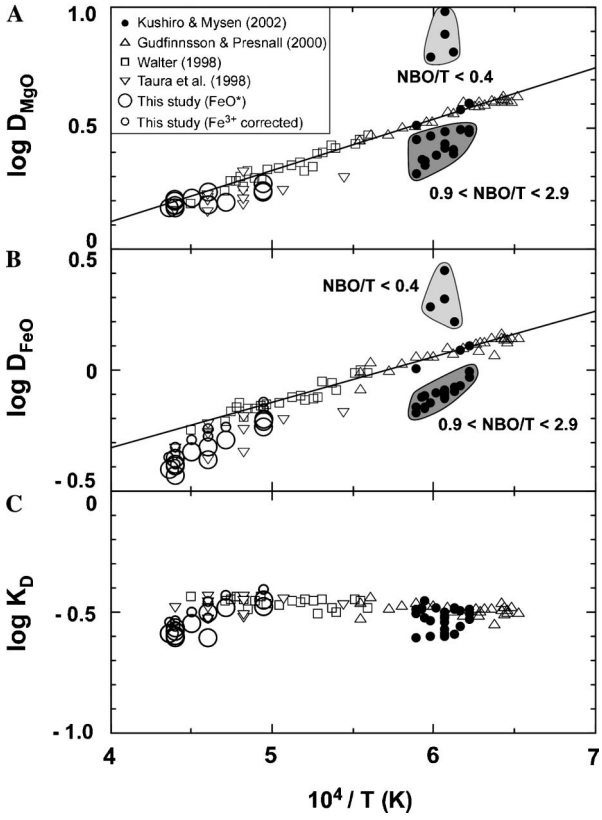

Fig. 7. Plots of: (A) $\log D_{MgO}$; (B) $\log D_{FeO}$; and (C) $\log K_D$ versus inverse temperature. The light-shaded and the dark-shaded areas in (A) and (B) indicate the melt compositions with NBO/T < 0.4 and 0.9 < NBO/T < 2.9, respectively (Kushiro and Mysen, 2002). Note that the data points by Gudfinnsson and Presnall (2000) and Walter (1998) show a linear relationship between inverse temperature and $\log D_{MgO}$ (solid line in (A): $\log D_{MgO} = 0.214 \times 10^4/T - 0.745$, $R = 0.991$) and $\log D_{FeO}$ (solid line in (B): $\log D_{FeO} = 0.187 \times 10^4/T - 1.072$, $R = 0.983$), whereas the data points by Kushiro and Mysen (2002) with NBO/T < 0.4 (light shaded) and 0.9 < NBO/T < 2.9 (dark shaded), Taura et al. (1998), and the present study deviate from these solid lines.

and the present study in Fig. 7A also show linear relationship between inverse temperature and $\log D_{MgO}$, consistent with the fact that D_{MgO} can be used as a geothermometer (Sugawara, 2000; Gudfinnsson and Presnall, 2001). However, the data points by Kushiro and Mysen (2002) with NBO/T < 0.4 and 0.9 < NBO/T < 2.9 in Figs. 7A and B, and those by Taura et al. (1998), and the present study in Fig. 7B deviate from the regression lines. The deviation from the linear relationship between inverse temperature and $\log D_{MgO}$, $\log D_{FeO}$, and $\log K_D$ indicates that the ratios of the activity coefficients $\gamma_L^{MgO}/\gamma_{ol}^{fo}$, $\gamma_L^{FeO}/\gamma_{ol}^{fa}$, and $\gamma_L^{MgO}/\gamma_L^{FeO}$ (γ_L^{MgO}, γ_L^{FeO}: activity coefficient for MgO and FeO in the liquid, γ_{ol}^{fo}, γ_{ol}^{fa}: activity coefficient for forsterite and fayalite in the olivine) change with composition (i.e., structure) of the liquid (Longhi et al., 1978). Toplis (2005) obtained the empirical equation to calculate K_D by estimating the effects of pressure, temperature, and composition on $\gamma_L^{MgO}/\gamma_L^{FeO}$ using thermodynamic formulations and large number of experimental data. Although the equation by Toplis (2005) predicts K_D very well up to about 10 GPa, it cannot reproduce K_Ds obtained in the present study at pressures from 10 to 13 GPa.

Kushiro and Mysen (2002) suggested that preference of Fe^{2+} and Mg^{2+} among the various types of non-bridging oxygen in the melts is reflected in the relationship between K_D and NBO/T of the melts, although how the preferences of Fe^{2+} and Mg^{2+} are related to particular types of structural units in melts at various pressure and temperature conditions is not known at present. In addition to the preferences of Fe^{2+} and Mg^{2+}, the possible structural change of ultramafic melts as a result of pressure-induced change in coordination of Si and Al (e.g., Xue et al., 1991; Lee et al., 2004) could be an important factor in understanding the origin of the relationship between K_D and NBO/T of the melts at high pressure and temperature conditions.

5. Implications

The negative correlation between pressure and K_D above 5 GPa suggests important implications for crystallization differentiation in the primordial terrestrial magma ocean and the origin of upper mantle peridotite, as well as the origin of ultramafic melts in the upper mantle (Kushiro and Walter, 1998). It has been suggested that olivine floatation can occur in magmas (e.g., Stolper et al., 1981; Agee and Walker, 1988a; Suzuki and Ohtani, 2003) at high pressures and could govern the chemical differentiation in the early Earth's interior (e.g., Ohtani, 1985; Agee and Walker, 1988b). To test this hypothesis, the composition of the liquidus olivine in peridotitic melt has been estimated based on $K_D = 0.38$ (Agee and Walker, 1988a; Suzuki and Ohtani, 2003). However, our experimental results indicate that the negative correlation between pressure and K_D should be taken into consideration. At 13 GPa, for example, $K_D = 0.25$–0.28 has to be used, which would result in the reduction of the depth of density crossover between peridotite melt and olivine.

Similarly, the primary magmas generated in the deep upper mantle such as komatiites must be more Fe-rich than that estimated previously. Komatiites are ultramafic lavas with >18% MgO and having spinifex textures (Kerr and Arndt, 2001). On the basis of experimental evidence, it is known that komatiites can be generated by melting of peridotite at pressures in the range of 3–15 GPa (e.g., Takahashi and Scarf, 1985; Walter, 1998; Herzberg and O'Hara, 1998). Barberton komatiites, which are thought to be deep origin (~10 GPa, Herzberg and O'Hara, 1998), have high FeO/MgO with high NBO/T ~ 2.4 (Nisbet et al., 1993). On the other hand, newly discovered Commondale komatiites (Wilson, 2003) have low FeO/MgO with low NBO/T ~ 1.7. This difference in FeO/MgO between these two types of komatiites might be related to the parabolic relationship between K_D and NBO/T.

A recent study of Gaetani (2004) shows that melt structure (i.e., NBO/T) also has a significant influence on the partitioning of trace elements between clinopyroxene and silicate melt. More detailed and systematic studies of the influence of melt structure on element partitioning between minerals and magmas, as well as studies of the structure of silicate melts at high pressures, have to be done for a better understanding of magmatism and chemical differentiation in the Earth's deep interior.

Acknowledgments

We thank S. Nakada and Y. Suzuki for their support in XRF measurements at ERI. We also thank S. Keshav for his helpful comments. Constructive, instructive, and careful reviews by G.H. Gudfinnsson, S. Parman, and M. Baker significantly improved the manuscript. This work was supported by the Research Fellowships of the Japan Society for the Promotion of Science for Young Scientists.

Associate editor: F.J. Ryerson

References

Agee, C.B., Walker, D., 1988a. Static compression and olivine floatation in ultrabasic silicate liquid. *J. Geophys. Res.* **93**, 3437–3449.

Agee, C.B., Walker, D., 1988b. Mass balance and phase density constraints on early differentiation of chondritic mantle. *Earth Planet. Sci. Lett.* **90**, 144–156.

Akaogi, M., Ito, E., Navrotsky, A., 1989. Olivine-modified spinel–spinel transitions in the system Mg_2SiO_4–Fe_2SiO_4: calorimetric measurements, thermochemical calculation, and geophysical application. *J. Geophys. Res.* **94**, 15671–15685.

Baker, M.B., Hirschmann, M.M., Wasylenki, L.E., Ghiorso, M.S., Stolper, E.M., 1995. Quest for low-degree mantle melts (Scientific Correspondence). *Nature* **381**, 286.

Bence, A.E., Albee, A.L., 1968. Empirical correction factors for the electron microanalysis of silicates and oxides. *J. Geol.* **76**, 382–403.

Chakraborty, S., Knoche, R., Schulze, H., Rubie, D.C., Dobson, D., Ross, N.L., Angel, R.J., 1999. Enhancement of cation diffusion rates across the 410-kilometer discontinuity in Earth's mantle. *Science* **283**, 362–365.

Ford, C.E., Russell, D.G., Graven, J.A., Fisk, M.R., 1983. Olivine-liquid equilibria: temperature, pressure and composition dependence of

crystal/liquid cation partition coefficients for Mg, Fe^{2+}, Ca and Mn. *J. Petrol.* **24**, 256–265.

Gaetani, G.A., 2004. The influence of melt structure on trace element partitioning near the peridotite solidus. *Contrib. Mineral. Petrol.* **147**, 511–527.

Gaetani, G.A., Grove, T.L., 1998. The influence of water on melting of mantle peridotite. *Contrib. Mineral. Petrol.* **131**, 323–346.

Gasparik, T., 1996. Melting experiments on the enstatite–diopside join at 70–224 kbar, including the melting of diopside. *Contrib. Mineral. Petrol.* **124**, 139–153.

Gee, L.L., Sacks, R.O., 1988. Experimental petrology of melilite nephelinites. *J. Petrol.* **29**, 1235–1255.

Gudfinnsson, G.H., Presnall, D.C., 2000. Melting behaviour of model lherzolite in the system CaO–MgO–Al_2O_3–SiO_2–FeO at 0.7–2.8 GPa. *J. Petrol.* **41**, 1241–1269.

Gudfinnsson, G.H., Presnall, D.C., A pressure-independent geothermometer for primitive mantle melts, J., 2001. *Geophys. Res.* **106**, 16205–16211.

Hamilton, D.H., Henderson, C.M.B., 1968. The preparation of silicate composition by a gelling method. *Mineral. Mag.* **36**, 832–838.

Herzberg, C.T., O'Hara, M.J., 1998. Phase equilibrium constraints on the origin of basalts, picrites, and komatiites. *Earth Sci. Rev.* **44**, 39–79.

Herzberg, C.T., Zhang, J., 1996. Melting experiments on anhydrous peridotite KLB-1: compositions of magmas in the upper mantle and transition zone. *J. Geophys. Res.* **101**, 8271–8295.

Irifune, T., Ohtani, E., 1986. Melting of pyrope $Mg_3Al_2Si_3O_{12}$ up to 10 GPa: possibility of a pressure-induced structural change in pyrope melt. *J. Geophys. Res.* **91**, 9357–9366.

Kerr, A.C., Arndt, N.T., 2001. A note on the IUGS reclassification of the high-Mg and picritic volcanic rocks. *J. Petrol.* **42**, 2169–2171.

Kushiro, I., 1996. Partial melting of a fertile mantle peridotite at high pressures: an experimental study using aggregates of diamond. In: Basu, A., Hart, S. (Eds.), *Earth Processes: Reading the Isotopic Code*. Am. Geophys. Union, pp. 109–122.

Kushiro, I., Walter, M.J., 1998. Mg–Fe partitioning between olivine and mafic–ultramafic melts. *Geophys. Res. Lett.* **25**, 2337–2340.

Kushiro, I., Mysen, B.O., 2002. A possible effect of melt structure on the Mg–Fe^{2+} partitioning between olivine and melt. *Geochim. Cosmochim. Acta* **66**, 2267–2272.

Lee, S.K., Cody, G.D., Fei, Y., Mysen, B.O., 2004. Nature of polymerization and properties of silicate melts and glasses at high pressure. *Geochim. Cosmochim. Acta* **68**, 4189–4200.

Lesher, C.E., Walker, D., 1988. Cumulate maturation and melt migration in a temperature gradient. *J. Geophys. Res.* **93**, 10295–10311.

Longhi, J., Walker, D., Hays, J.F., 1978. The distribution of Fe and Mg between olivine and lunar basaltic liquids. *Geochim. Cosmochim. Acta* **42**, 1545–1558.

Matsukage, K.N., Kubo, K., 2003. Chromian spinel during melting experiments of dry peridotite (KLB-1) at 1.0–2.5 GPa. *Am. Mineral.* **88**, 1271–1278.

Mibe, K., Yoshino, T., Ono, S., Yasuda, A., Fujii, T., 2003. Connectivity of aqueous fluid in eclogite and its implications for fluid migration in the Earth's interior. *J. Geophys. Res.* **108**, B6. doi:10.1029/2002JB001960.

Miyajima, N., Langenhorst, F., Frost, D.J., Yagi, T., 2004. Electron channelling spectroscopy of iron in majoritic garnet and silicate perovskite using a transmission electron microscope. *Phys. Earth Planet. Inter.* **143–144**, 601–609.

Morishima, H., Kato, T., Suto, M., Ohtani, E., Urakawa, S., Utsumi, W., Shimomura, O., Kikegawa, T., 1994. The phase boundary between α- and β-Mg_2SiO_4 determined by in situ X-ray observation. *Science* **265**, 1202–1203.

Mysen, B.O., Virgo, D., Seifert, F.A., 1982. The structure of silicate melts: implications for chemical and physical properties of natural magma. *Rev. Geophys. Space Phys.* **20**, 353–383.

Nakada, S., 1997. Origin of phenocrysts and eruption mechanism—in case of of Unzen Volcano. Report of Grant-in-Aid for Scientific Research (B) No. 07454134, 45p.

Nisbet, E.G., Cheadle, M.J., Arndt, N.T., Bickle, M.J., 1993. Constraining the potential temperature of the Archaean mantle: a review of the evidence from komatiites. *Lithos* **30**, 291–307.

Ohtani, E., 1985. The primordial terrestrial magma ocean and its implications for stratifications of the mantle. *Phys. Earth Planet. Inter.* **38**, 70–80.

O'Neill, H.S.C., Eggins, S.M., 2002. The effect of melt composition on trace element partitioning: an experimental investigation of the activity coefficients of FeO, NiO, MoO_2 and MoO_3 in silicate melts. *Chem. Geol.* **186**, 151–181.

Ono, S., 1998. Stability limits of hydrous minerals in sediment and mid-ocean ridge basalt compositions: implications for water transport in subduction zones. *J. Geophys. Res.* **103**, 18253–18267.

Ringwood, A.E., 1966. The chemical composition and origin of the Earth. In: Hurley, P.M. (Ed.), *Advances in Earth Science*. Massachusetts Institute of Technology Press, Cambridge, Massachusetts, USA, pp. 287–356.

Roeder, P.L., Emslie, R.F., 1970. Olivine–liquid equilibrium. *Contrib. Mineral. Petrol.* **29**, 275–289.

Stolper, E., Walker, D., Hager, B.H., Hays, J.F., 1981. Melt segregation from partially molten source regions: the importance of melt density and source region size. *J. Geophys. Res.* **86**, 6261–6271.

Sugawara, T., 2000. Empirical relationship between temperature, pressure, and MgO content in olivine and pyroxene saturated liquid. *J. Geophys. Res.* **105**, 8457–8472.

Suzuki, A., Ohtani, E., 2003. Density of peridotite melts at high pressure. *Phys. Chem. Miner.* **30**, 449–456.

Takahashi, E., 1978. Partitioning of Ni^{2+}, Co^{2+}, Fe^{2+}, Mn^{2+} and Mg^{2+} between olivine and silicate melts: compositional dependence of partition coefficient. *Geochim. Cosmochim. Acta* **42**, 1829–1844.

Takahashi, E., 1986. Melting of a dry peridotite KLB-1 up to 14 GPa: implications on the origin of peridotitic upper mantle. *J. Geophys. Res.* **91**, 9367–9382.

Takahashi, E., Kushiro, I., 1983. Melting of a dry peridotite at high pressures and basalt magma genesis. *Am. Mineral.* **68**, 859–879.

Takahashi, E., Scarf, C.M., 1985. Melting of peridotite to 14 GPa and the genesis of komatiite. *Nature* **315**, 566–568.

Taura, H., Yurimoto, H., Kurita, K., Sueno, S., 1998. Pressure dependence on partition coefficients for trace elements between olivine and the coexisting melts. *Phys. Chem. Miner.* **25**, 469–484.

Toplis, M.J., 2005. The thermodynamics of iron and magnesium partitioning between olivine and liquid: criteria for assessing and predicting equilibrium in natural and experimental systems. *Contrib. Mineral. Petrol.* **149**, 22–39.

Ulmer, P., 1989. The dependence of the Fe^{2+}–Mg cation-partitioning between olivine and basaltic liquid on pressure, temperature and composition. *Contrib. Mineral. Petrol.* **101**, 261–273.

Walter, M.J., 1998. Melting of garnet peridotite and the origin of komatiite and depleted lithosphere. *J. Petrol.* **39**, 29–60.

Wilson, A.H., 2003. A new class of silica enriched, highly depleted komatiites in the southern Kaapvaal Craton, South Africa. *Precambrian Res.* **127**, 125–141.

Xirouchakis, D., Hirschmann, M.M., Simpson, J.A., 2001. The effect of titanium on the silica content and on mineral–liquid partitioning of mantle-equilibrated melts. *Geochim. Cosmochim. Acta* **65**, 2201–2217.

Xue, X., Stebbins, J.F., Kanzaki, M., McMillan, P.F., Poe, B., 1991. Pressure-induced silicon coordination and tetrahedral structural change in alkali oxide–silica melts up to 12 GPa: NMR, Raman, and infrared spectroscopy. *Am. Mineral.* **76**, 8–26.